Contrib Mineral Petrol (1996) 125: 100–111

G.R. Watt · I.M. Burns · G.A. Graham

Chemical characteristics of migmatites: accessory phase distribution and evidence for fast melt segregation rates

Received: 12 July 1995 / Accepted: 4 March 1996

Abstract Equilibration between melt and solid is inhibited by rapid melt extraction and by restricted equilibration (armouring, slow dissolution). When segregation occurs by channelised migration along high-porosity pathways, melt migration is more rapid than trace element diffusion rates in silicates and faster than accessory phase dissolution rates. Evidence for channelised flow and deformation-enhanced melt segregation into boudin necks, fractures and micro-shears at low melt fractions is present in the Moine Kirtomy Migmatitie Suite (KMS) in Sutherland, Scotland. Melt migration distances are on a metre to tens of metres scale. Concordant leucosomes in stromatic migmatities in the KMS have low Zr contents, low LREE (light rare-earth element) and H (heavy) REE contents and positive Eu anomalies. REE patterns of this type can be produced by removal of leucosome before complete equilibration with source due to the inhibited dissolution of LREE- and HREE-bearing accessory phases in water-undersaturated melts. Melting in the KMS, however, occurred at or near the wet granite solidus, leaving biotite as a residual phase. Detailed back-scattered electron imaging shows that REE-bearing accessory phases remained as residual phases, and were concentrated in the melanosome and at the melanosome-leucosome boundary. Irregularly shaped patches of diatexite contain a small proportion of excess Zr, consistent with entrainment of melanosome-schlieren enriched in zircon. These data indicate that deformation-enhanced melt extraction led to the rapid migration of small melt fractions from the melting site on a time-scale less than that required to saturate the melt in Zr. Leucosomes were thus prevented from equilibrating with accessory phases before extraction.

G.R. Watt (✉) · I.M. Burns
Geology and Cartography Division, SCES,
Oxford Brookes University, Headington, Oxford, OX3 0BP, UK

G.A. Graham
The Open University, Walton Hall, Milton Keynes, MK7 6AA, UK

Editorial responsibility: I. Parsons

Introduction

Disequilibrium melting occurs when melts are removed from melting source rocks before the liquid has completely equilibrated with the solid assemblage of the residue. The extent to which equilibrium is attained depends upon the relative rates of melt segregation and melt-solid dissolution/partitioning. Recent compilations of melt segregation rates (Paterson and Tobisch 1992) show that granitic melt velocities (10^{-7} to 10^{-8} cm^2s^{-1}) are more rapid than diffusion velocities in silicates (10^{-10} to 10^{-18} cm^2s^{-1}), although these are strongly dependent upon melt viscosity (Brown et al. 1995a). Once segregation into high-porosity pathways (e.g. veins) occurs then melt migration rates may be several orders of magnitude faster still (Bedard 1989; Brown 1994a). Evidence for channelised flow and deformation-enhanced melt segregation (e.g. Brown 1994a, Brown et al. 1995b) on a hand specimen and outcrop scale (boudin necks, veins, melt migration into micro-shears) is present in most migmatities (e.g. McLellan 1988; Pattison and Harte 1988) where melt migration occurs over a variety of distances. Equilibration between melt and solid can also be limited by armouring of phases in residual material, thus isolating them from the melt (Bea et al. 1994; Nabelek and Glascock 1995), or by kinetic effects such as the restricted dissolution of zircon, monazite and apatite in water-undersaturated granitic melts (Watt and Harley 1993).

Most petrogenetic modelling of melting systems assumes that chemical equilibrium is attained between the solid and melt phases during anatexis. If melts segregate from their sources by a combination of short-range grain-scale movement and longer range channelized flow, then the widespread assumption that melt-source equilibration occurs before melt extraction becomes questionable. One model which considers the effects of slow diffusion in silicates and restricted equilibration is the "Carrier Mineral Model" of Bea (1991). In this model melt migration is rapid and effective distribution coef-

ficients approach unity – *no* chemical partitioning between solid and melt occurs and melt chemistry is determined solely by the chemical compositions of the melting phases in the source (Ashworth and Brown 1990). Under less extreme conditions, where melt partially equilibrates with the crystalline matrix before extraction, variation in rates at which solid-melt partitioning and partial dissolution of melting phases proceed allows the formation of a wide spectrum of melt compositions from a single source. This will be particularly true in melt-solid systems where segregation and separation of melts is rendered more effective by deformation (Sawyer 1994). The liquid composition generated is controlled by the mode of the source, diffusion rates for each chemical species between melt and solid, the melting rate of each phase (including accessory phases), the rate of melt-solid equilibration and partitioning of elements between solid and melt (relative to the rate of melt removal) and the length scale of melt extraction.

Geochemical evidence for the removal of partially equilibrated melt has been recorded in mantle peridotites (Bedard 1989; Qin 1992; Iwamori 1994), contact aureoles (Naslund 1986), metabasic migmatites (Sawyer 1991) and peltic migmatites (Srogi et al. 1993; Watt and Harley 1993). Crustal source rocks, especially those of pelitic or semi-pelitic composition, contain higher proportions of accessory phase minerals (with reference to zircon, monazite and apatite) than mantle lithologies. The important role of these accessory phases in influencing melt chemistry during partial melting has been recognised by many workers (Sawyer 1991; Watt and Harley 1993; Harris et al. 1994). Using the empirical equations of Watson (1988) and Montel (1993) it is possible to calculate concentrations of zirconium (Zr*) and the light rare-earth elements La–Gd (LREE*) in equilibrium melts. Equilibrium liquids will have $Zr_{(measured)}$/Zr* and $LREE_{(measured)}$/LREE* values of unity, while melts with values less than 1.0 have disequilibrium compositions. Sawyer (1991) suggested small-volume leucosomes in amphibolite-facies migmatites had disequilibrium compositions ($Zr/Zr^* < 1.0$) because they were formed at low temperatures which restricted zircon dissolution, while Watt and Harley (1993) ascribed low Zr and LREE concentrations in granulite-facies leucosomes to restricted accessory phase dissolution in water-undersaturated melts. One of the outcomes of the limited dissolution of accessory phases during melting is the complementary enrichment of accessory phases in the residue. The principal geochemical consequences of rapid melt migration in crustal lithologies, therefore, are the strong enrichment of highly "incompatible" elements in the residue (compared to concentrations predicted by equilibrium, batch or fractional melting models) and a corresponding depletion in the melt. Conversely, extremely rapid melting of accessory phases in mantle peridotites may strongly enrich LILE (large-ion lithophile elements) and LREE concentrations in first-formed melt compositions (Campbell and Gorton 1980; Watson and Harrison 1983). Accessory phases, therefore, provide us with useful geochemical and petrographic markers with which to measure how effectively melt and restite have equilibrated before melt removal.

Pelitic and semi-pelitic lithologies represent the most likely protolith for the generation of peraluminous granites (Clemens 1990; Clemens and Vielzeuf 1987; Miller 1985; Patiño Douce and Johnston 1991), so an understanding of melt extraction rates may allow us to make important deductions regarding the time scales of partial melting events, melt extraction and the potential depth of generation of granites. In this paper we describe and interpret the petrographic and geochemical features of partial melting in pelitic and semi-pelitic lithologies from amphibolite-facies migmatites in the Kirtomy Nappe in Sutherland, Scotland. We present field and petrographic observations, major and trace element (including rare-earth element) bulk rock and mineral analyses and back-scattered electron and cathodoluminescence images of accessory phases which allow us to suggest that melt extraction in the Kirtomy Migmatite Suite (KMS) occurred rapidly. Melt extraction occurred before equilibration with source lithologies, due to a combination of low anatectic temperatures and deformation-enhanced melt segregation at low melt fractions.

Geological setting and lithologies studied

Geological setting

This study is focused on the geochemical and petrographic features of a suite of migmatites exposed in the Kirtomy Nape (Fig. 1). The Kirtomy nappe forms the structurally highest unit of a series of east-dipping Caledonian (Ordovician–Silurian) thrust nappes exposed along the north coast of Sutherland, Scotland (Holdsworth et al. 1995). The lower part of the nappe pile consists of lower-amphibolite-facies Moine rocks of the Moine Nappe bounded to the west by the Moine Thrust Zone. Overlying the Moine Nappe is the Naver Nappe, which is dominated by middle-amphibolite-facies Moine gneisses and metatexitic migmatities, and contains several inliers of Lewisian basement rocks. The Kirtomy Nappe occurs structurally above the Kirtomy Thrust and contains two distinct rock units, the Kirtomy Migmatite Suite (KMS) and the Strathy Complex (Burns 1994). The KMS is exposed between Kirtomy and Port Mor (east of Ardmore Point), and forms a thick sequence of diatexitic and metatexitic migmatites, relict semi-pelitic gneiss and subordinate orthogneiss. Migmatites range from regularly layered stromatic types to disrupted, diatexitic areas up to 200 m^2. Two main types of leucosome have been distinguished on the basis of their relationships with layering. Concordant leucosomes in stromatic migmatites form layers of quartzofeldspathic composition up to 10 cm thick and 5–10 m lateral extent. Lithologically similar leucosomes have been recorded in the axial zones of folds and small shear zones. Patches and veins of leucosome material discordant to layering also occur (discordant leucosomes) – some are relatively coarse grained to pegmatitic and contain little or no mafic material and others are more diatexitic. The diatexitic leucosomes contain schlieren of biotite and xenoliths of psammitic, semi-pelitic and pelitic gneiss. Xenoliths of variably migmatised semi-pelitic, pelitic and psammitic gneiss are common in larger areas of diatexitic material.

The stability of biotite throughout melting indicates that melting occurred on or slightly above the vapour-present biotite-granite solidus (Vielzeuf and Holloway 1988) – muscovite is absent in all samples. *P–T* estimates for amphobilite layers within the KMS

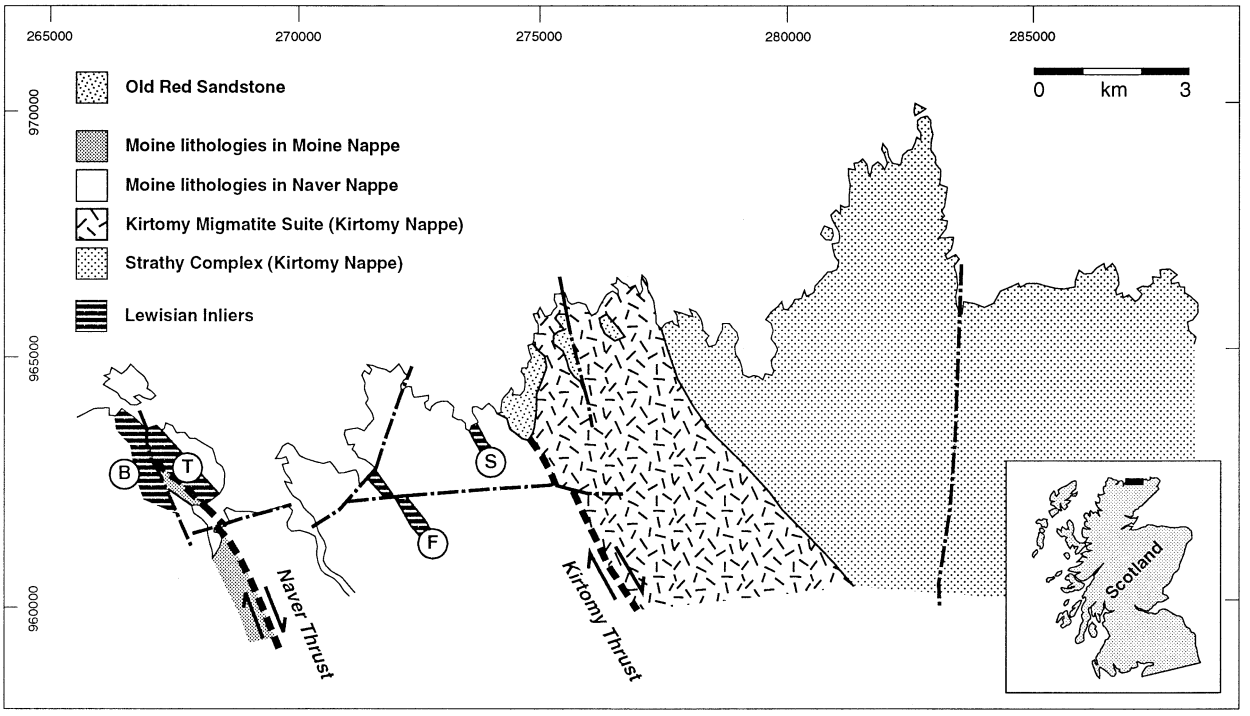

Fig. 1 General geology of the area around Bettyhill, Sutherland, NW Scotland showing the location of the Kirtomy Migmatite Suite. (Key to Lewisian Inliers: *B* Borgie, *T* Torrisdale, *F* Farr, *S* Strathy) Numbers on the border are National Grid coordinates

using garnet-hornblende (Graham and Powell 1984) and amphibole-plagioclase (Holland and Blundy 1994) thermometry and garnet-hornblende-plagioclase-quartz barometry (Kohn and Spear 1990) give peak metamorphic conditions of 700–720° C, 4.5–5.5 kbar. Three deformation episodes have been recognised in the Kirtomy Nappe. The D1 fabrics are tentatively correlated with Grenvillian (c1000 Ma) deformation. The D2 (early Caledonian) deformation involved W to NW ductile thrusting and nappe juxtaposition, and was accompanied by upper-greenschist/lower-amphibolite-facies conditions in the Naver Nappe and upper-amphibolite-facies migmatisation in the Kirtomy Nappe. Foliation and fold trends in the Kirtomy Migmatites either conform to regional patterns (segregation banding shows a dominant foliation trend N–NNW) or are anomalous due to melt movement. The D2 folds in the Kirtomy migmatites are close to tight, upright to inclined folds on a centimetre to metre scale. Axial planar fabrics are rarely developed, but can be picked out occasionally by leucosome segregations (Fig. 2). Axial surface trends dip sub vertically between west and south. Many folds are disrupted due to melt migration along and across fold limbs and noses – where leucosome accumulation has occurred fold noses only are preserved (Burns 1994). Melting occurred synchronously with D2 (Caledonian) deformation – segregation banding defines F2 folds which in turn are cut by leucosome veins and pools but these leucosome structures are also deformed by D2 structures. Recrystallisation of D2 fabrics and mineral assemblages occurred along the Naver and Kirtomy thrusts. Finally, late/post D3 static annealing under lower-amphibolite-facies conditions is recorded throughout the Naver and Kirtomy Nappes.

Analytical procedures

Detailed petrographic and geochemical analysis of a suite of leucosomes in stromatic migmatites (SL), pegmatitic leucosomes (PDL), diatexitic leucosomes (DL), and melanosomes (MEL) from the Kirtomy Migmatite suite are reported. Samples with the prefix KM-93 were collected by G.A.G., and those with the prefix KM-94 by G.R.W. Major element mineral compositions were determined on a JEOL JSM-840 scanning electron microscope fitted with LINK E-XL X-ray energy dispersive spectroscopy software at the Department of Geology, Oxford Brookes University. Analyses were performed at an accelerating voltage of 20 kV and a beam current of 2 nA. Correction for matrix effects were made using an on-line ZAF correction package. Trace element concentrations in biotite, plagioclase, K-feldspar and zircon were determined on a Cameca ims-4f ion microprobe at the University of Edinburgh. An O^- primary beam with an accelerating voltage of -10 keV was produced by a duoplasmatron gun giving a net impact energy at the sample of 14.5 keV. Primary beam current was 8 nA producing a spot size of approximately 20–30 µm. An energy window of ± 19 eV and an energy offset of 100 eV were used. Molecular species were reduced using energy filtering methods as described in Zinner and Crozaz (1987) and Hinton (1990). Analysis of the following isotopes were carried out; ^{30}Si, ^{85}Rb, ^{88}Sr, ^{89}Y, ^{90}Zr, ^{93}Nb, ^{138}Ba, ^{139}La, ^{140}Ce, ^{143}Nd, ^{147}Sm, ^{151}Eu, ^{157}Gd, ^{159}Tb, ^{161}Dy, ^{165}Ho, ^{167}Er, ^{169}Tm, ^{172}Yb and ^{175}Lu. Rubidium was corrected for the molecular FeSi peak at mass 84. Niobium was corrected for the presence of $^{92}ZrH^+$ by measurement of the $^{94}ZrH^+$ peak at mass 95 (Hinton 1990; Hinton and Upton 1991). Determination of both LREE and H (heavy) REE concentrations required correction for BaO, while HREE abundances were corrected for LREE. Trace element abundances were calculated relative to Si (determined by electron microprobe analysis) and calibrated against glass standard NBS610.

Migmatite samples were slabbed into 2–3 cm thick sections. These were then cut into strips approximately 2–3 cm×2–3 cm×10–20 cm. From these strips, leucosome and melanosome components were sampled using a fine saw. The samples were then crushed to 250 µm. Aliquots for whole rock analysis were then selected by cone and quarter reduction of an original sample of between 0.25 and 1 kg in weight. Major and rare-earth elements were analysed on a ARL 3510 ICPAES at Oxford Brookes University, after fusion dissolution and cation-exchange pre-concentration. Natural multi-element rare-earth standards were used following the methodology of Watkins and Nolan (1992). Accuracy was monitored with international reference materials, precision by

Fig. 2 **a** Typical deformed stromatic Kirtomy migmatites. Alternating bands of pale white leucosome, dark grey mesosome and quartz-rich "melanosome" and black, biotite-rich melanosome folded into tight "M" and "W" profiles showing incipient development of leucosome along fold limbs and axial surfaces. Note the discordant leucosome *left* of the hammer which cross-cuts banding in the stromatic migmatites. **b** Competent psammitic gneisses exhibiting small leucosome filled shear zones

replicate analyses. Both are estimated at better than ±2% for major element oxides and ±5% for trace elements.

Petrography

Migmatite mineralogies are simple and consistent over the spectrum of textures observed. Mesosome consists of medium- to coarse-grained semi-pelitic (rarely pelitic) gneiss comprised of quartz+plagioclase+K-feldspar+biotite±muscovite±garnet +zircon+monazite±apatite±fibrolite and secondary chlorite. Quartz often occurs as ribbons parallel to biotite defining the main foliation. Xenoblastic garnet rarely exceeds 0.2 mm in diameter, is unretrogressed and includes biotite laths parallel to the main migmatite fabric. Pelitic gneiss locally preserves an early fabric of fibrolite and biotite, overgrown by later biotite.

In stromatic migmatites, melanosomes are well-defined, coarse-grained layers up to a few cm thick, laterally continuous and parallel to leucosomes. Biotite in the melanosomes is coarser than biotite in the mesosome (2–3 mm long as opposed to 0.5–1 mm long). Irregular, partially disaggregated melanosome schlieren may be incorporated in the leucosome. Melanosome consists of quartz+plagioclase+K-feldspar+biotite+zircon+ apatite+monazite+ilmenite. Blue-grey quartz-rich residual selvedges form distinctive bands parallel to leucosomes. They are coarse-grained layers comprised almost entirely of quartz and biotite with rare plagioclase; apatite and abundant zircon and monazite are obvious in thin section. Quartz forms ribbons up to 2 cm long, parallel to the main migmatite layering.

Leucosomes are coarse grained, white/pink coloured and can be classified using a two-fold division based on relations with surrounding banded gneisses – they are either concordant or discordant to local foliation. Most common are layer parallel concor-

dant leucosomes in stromatic migmatites up to 5 cm thick, flanked by biotite- or quartz-rich selvedges. As leucosome proportion increases, intrusive relationships with the surrounding host gneisses become more apparent – leucosome veins and pods truncate layering and fold structures at high angles. Leucosome-filled shear zones and fold axial planes are common (Fig. 2). Discordant leucosomes can either be coarse grained and biotite free (pegmatitic leucosomes) or diatexitic. The more homogeneous, schlieren-free diatexites have a coarse-grained granular texture and the following assemblage; quartz+plagioclase+K-feldspar+biotite+muscovite+zircon+monazite+apatite+ore±chlorite. Mesosome, melanosome and leucosome plagioclase in stromatic migmatites is identical in composition, and consists of andesine cores (X_{an}=0.29–0.32) with narrow albite (X_{an}=0.02–0.10) rims. The narrow (5–20 μm) Na-enriched rim was interpreted as a late stage alteration by Burns (1994) and probably reflects down temperature re-equilibration of plagioclase. The lack of fractionation of plagioclase between melanosome and mesosome during partial melting (Johannes 1978, 1980) has been used as evidence for disequilibrium melting by several authors (e.g. Srogi et al. 1993), and occurs due to the slow approach of plagioclase to equilibrium liquidus compositions – the net geochemical effect is that of stoichiometric melting of plagioclase (Ashworth and Brown 1990; Johannes 1980). Biotite occurrence is interpreted as the re-distribution of relict grains or clots of grains derived from entrainment of melanosome, rather than a mineral which has crystallised from the melt.

Bulk rock geochemistry

Both concordant and discordant leucosomes (Table 1) have restricted SiO_2 concentrations (72.22–75.16 wt%, with the exception of KM-94-4 which contains 79.49 wt% SiO_2), relatively high Al_2O_3 concentrations and molecular $Al_2O_3/CaO+Na_2O+K_2O$ (A/CNK) values of between 1.08 and 1.33, making them weakly to moderately peraluminous in the classification of Miller (1985). Both stromatic and ponded leucosomes are corundum normative (up to 4 wt%), and K_2O is greater than Na_2O in almost all samples. Major element chemistries are very similar to Himalayan leucogranites (France-Lanord and Le Fort 1988), cordierite- and garnet-bearing granites from the Hercynian Belt of Europe (Holtz 1989), experimental melt compositions (Carrington and Watt 1995) and leucosomes from other pelitic migmatites (Weber et al. 1985; Barbey et al. 1990). The field relationships of the leucosomes, restricted SiO_2 concentrations and the similarity with major element compositions reported from granitic compositions in the literature all suggest that leucosomes in the Kirtomy Migmatite Suite were derived by partial melting of a metasedimentary source (Miller 1985; White 1990).

Concordant and discordant leucosomes in the KMS have flat to moderately fractionated REE patterns (chondrite normalised, $La_{(N)}/Yb_{(N)}$=4.96–38.22), moderate to large positive Eu anomalies (Eu/Eu*=1.66) and low HREE abundances (Fig. 3). Positive Eu anomalies suggest disequilibrium melting of feldspar coupled with retention of LREE- and HREE-bearing accessory phases in the residuum (e.g. Watt and Harley 1993; Carrington and Watt 1995; Nabelek and Glascock 1995). Leucosomes in stromatic migmatites have lower absolute abundances of LREE (La–Gd) than discordant leucosomes

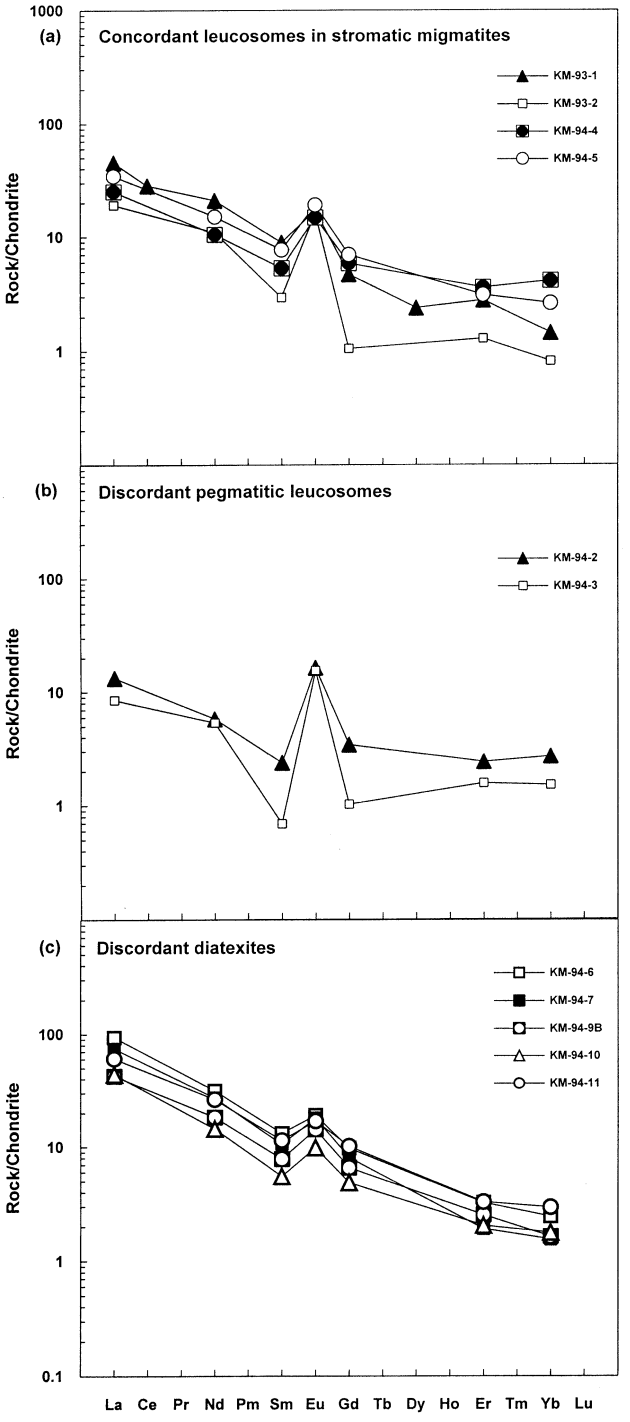

Fig. 3a–c Chondrite normalised rare-earth-element plots for: **a** concordant leucosomes in stromatic migmatites; **b** discordant leucosomes (pegmatitic facies); **c** diatexites (containing biotite). Note the higher HREE contents and smaller positive Eu anomalies in the diatexitic leucosomes reflecting progressive entrainment of host material

containing biotite, suggesting that these discordant leucosomes may contain some entrained LREE-bearing material. The LREE saturation calculations were carried out for the KMS using the equations of Montel (1993). Calculations used *P–T* conditions of 700° C, 5 kbar (Burns,

Table 1 Bulk rock geochemistry – Kirtomy Migmatite Suite (*CL* Concordant leucosome, *PDL* discordant leucosome, pegmatitic, *DL* discordant diatexite, *MEL* melanosome, *LOI* loss on ignition)

	KM-93-1 CL	KM-93-2 CL	KM-93-3 MEL	KM-93-4 MEL	KM-94-2 PDL	KM-94-3 PDL	KM-94-4 CL	KM-94-5 CL	KM-94-6 DL	KM-94-7 DL	KM-94-9A MEL	KM-94-9B DL	KM-94-10 DL	KM-94-11 DL
SiO_2	73.03	73.04	48.19	35.99	73.36	75.40	79.49	75.16	72.22	73.79	80.34	74.08	75.00	75.00
TiO_2	0.11	0.11	2.80	3.49	0.05	0.11	0.05	0.08	0.20	0.16	1.19	0.23	0.15	0.14
Al_2O_3	16.01	15.80	15.21	18.23	14.98	14.67	11.41	13.12	14.95	14.65	5.64	13.62	14.22	13.78
Fe_2O_3	0.90	0.86	17.24	23.42	0.50	0.80	0.50	0.56	1.30	1.04	6.64	1.62	0.96	0.96
MnO	0.01	0.01	0.36	0.34	0.01	0.01	0.01	0.02	0.02	0.02	0.07	0.02	0.02	0.02
MgO	0.25	0.23	5.07	6.86	0.25	0.26	0.25	0.25	0.55	0.36	1.91	0.64	0.26	0.32
CaO	1.46	1.53	0.73	2.55	2.20	2.31	2.31	0.75	1.47	1.29	0.41	1.84	0.81	1.69
Na_2O	3.72	4.09	0.42	0.00	2.48	0.94	0.61	6.88	3.61	4.19	2.66	1.09	4.76	2.86
K_2O	5.28	4.69	7.31	9.46	4.73	5.19	3.86	2.25	4.11	3.91	0.10	4.72	4.07	3.91
P_2O_5	0.06	0.05	0.37	0.19	0.10	0.10	0.10	0.10	0.10	0.10	0.29	0.10	0.10	0.10
LOI	0.23	0.32	0.92	1.02	0.31	0.49	0.46	0.39	0.41	0.29	0.54	0.60	0.56	0.57
Total	101.06	100.73	98.62	101.55	98.97	100.28	99.05	98.94	98.94	99.80	99.79	98.56	100.91	99.35
A/CNK[a]	1.11	1.08	1.53	1.23	1.14	1.29	1.22	1.15	1.15	1.09	1.08	1.33	1.04	1.15
Zr	38	57	695	648	63	116	9	130	130	117	624	103	84	113
La	14.95	6.3	93.00	48.77	4.39	2.81	8.28	30.96	30.96	24.54	82.34	14.07	14.53	20.02
Ce	24.46	5.6	177.00	91.39	5.68	5.77	12.92	49.38	49.38	40.89	153.70	24.78	22.77	35.56
Nd	13.21	6.87	86.70	46.07	3.65	3.37	6.61	9.50	19.88	17.16	71.30	11.55	9.13	16.61
Sm	1.81	0.6	16.10	8.94	0.48	0.14	1.08	1.56	2.69	2.14	12.36	1.59	1.12	2.32
Eu	1.32	1.24	1.30	0.60	1.25	1.18	1.14	1.47	1.47	1.39	1.02	1.10	0.76	1.31
Gd	1.29	0.29	14.40	8.69	0.94	0.28	1.61	1.91	2.68	2.22	11.76	1.81	1.34	2.79
Dy	0.82	0.74	9.20	5.67	1.12	0.85	2.26	1.86	1.89	1.85	7.84	2.17	1.92	3.69
Er	0.63	0.29	6.36	3.25	0.54	0.35	0.81	0.70	0.73	0.43	3.84	0.57	0.46	0.74
Yb	0.32	0.18	5.51	4.30	0.59	0.33	0.91	0.58	0.54	0.34	3.35	0.36	0.39	0.65
La (N)/ Yb(N)[b]	31.15	23.33	11.25	7.56	4.95	5.68	6.06	13.10	38.22	48.12	16.39	26.06	24.84	20.53
Eu/Eu*[c]	2.52	8.03	0.26	0.21	5.61	17.95	2.65	2.61	1.66	1.94	0.26	1.98	1.90	1.58

[a] Molecular $Al_2O_3/CaO+Na_2O+K_2O$
[b] Chondrite normalised value
[c] Eu anomaly

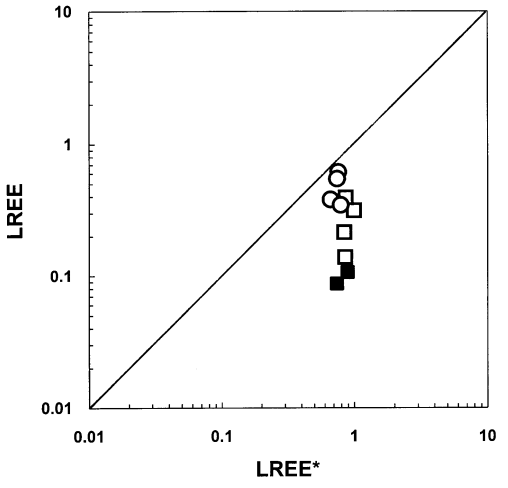

Fig. 4 Plot of LREE (La–Gd total measured) versus LREE* (La–Gd total calculated using the equations of Montel, 1993; 6 wt% H_2O and a temperature of 700° C were assumed – see text). (*Open squares* concordant leucosomes in stromatic migmatites, *filled squares* discordant pegmatitic leucosomes, *open circles* discordant diatexites)

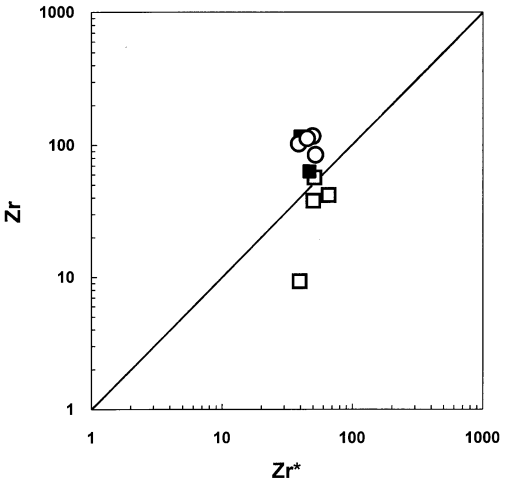

Fig. 5 Plot of Zr (measured) versus Zr (calculated using the equations of Watson, 1988, assuming a temperature of 700° C). (Symbols as Fig. 4)

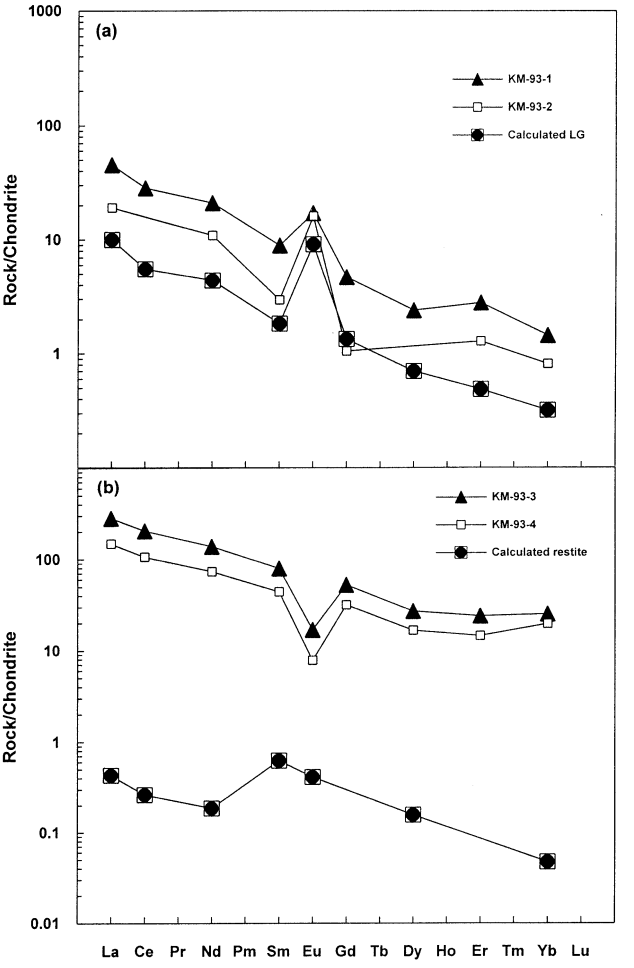

Fig. 6a, b Mass balance calculations: **a** Calculated leucosome composition (*dotted square symbol*) using recast quartz plagioclase, K-feldspar and biotite SIMS ion-probe data (G. Watt, unpublished). Also plotted are leucosomes in stromatic migmatites KM-93-1 and KM-93-2 for comparison. Note the similar fractionation and size/sign of the Eu anomalies. **b** Mass balance calculations for melanomes (recast as above). The difference between observed (KM-94-3, KM-94-4) and calculated REE profiles reflects the contribution of accessories – the modelled profile only considers quartz (essentially REE-free) and biotite

1994 and unpublished data), and a melt water content of 6% derived from the experimental data of Holtz and Johannes (1994) assuming that melting occurred at the wet solidus (biotite stable throughout melting). Figure 4 shows that stromatic, pegmatitic and diatexitic leucosomes are undersaturated with respect to LREE. Schlieren-rich diatexites are least undersaturated in LREE again consistent with entrainment of monazite or apatite, while pegmatitic leucosomes show the highest degree of undersaturation. This may reflect the fractionation of feldspars or LREE-bearing phases, or the removal of LREE in a late stage fluid as the final crystallisation of the melt occurred. In contrast, a plot of Zr/Zr* (Fig. 5) (calculated using the equations of Watson 1988) shows that leucosomes in stromatic migmatites, which have exceptionally low Zr concentrations of less than 50 ppm, are undersaturated in zircon while pegmatitic and diatexitic leucosomes have Zr/Zr* values greater than 1.0. The excess Zr in diatexitic leucosomes is probably of entrained origin (zircon is common as inclusions in biotite schlieren) and the apparent excess in pegmatitic leucosomes may be explained if (as is probable) these melts had a higher water content than the 6% estimates for the other leucosomes. Melts can dissolve more Zr as H_2O increases – the additional water present in the pegmatites would mean they are also undersaturated. The equation of Watson (1988) does not contain a term for H_2O so it is not possible to test this.

Fig. 6 shows the results of a simple REE mass balance calculation for leucosomes in stromatic migmatites. Ion

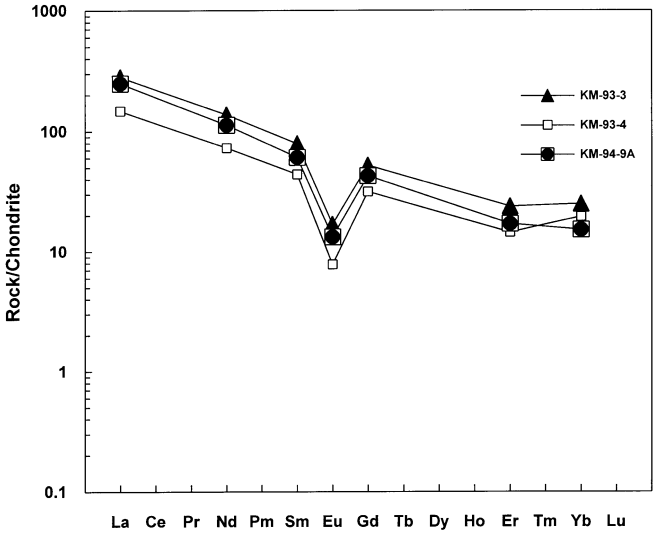

Fig. 7 Chondrite normalised REE plots for Melanosomes

probe data for the major phaes present are available from the authors. These data were recast in terms of modal proportions for a typical stromatic leucosome, and show a good correlation with observed REE plots from KMS leucosomes in stromatic migmatites. This correlation indicates that the bulk of the REEs present in the leucosomes in stromatic migmatites are hosted in plagioclase and K-feldspar, rather than accessory phases, consistent with the observations presented above which show that accessory phases are essentially absent from leucosomes in stromatic migmatites.

Melanosomes in the KMS have REE patterns which reflect their high modal abundances of zircon, apatite and monazite. The Zr contents are almost six times greater than leucosomes in stromatic migmatites. The LREE and HREE abundances are also greater than leucosomes, and Eu anomalies are large and negative ($Eu/Eu^* < 0.30$) (Fig. 7). Ion probe work and published data show quartz and biotite have very low REE contents, and mass balance calculations confirm that the majority of the LREE and HREE must reside in accessory phases which are concentrated in the melanosome.

Accessory phase distribution and controls on melt chemistry

In an attempt to determine the role that restricted zircon dissolution plays in the generation of Zr depleted leucosomes in stromatic migmatites, a detailed back-scattered electron and cathodoluminescence study of zircon morphology and distribution was carried out on two stromatic migmatite samples. Three distinctive zircon morphologies were identified:

Type A. Elongate prisms up to 200 μm long with aspect ratios greater than 2.0. Zoning is oscillatory and regular, and no truncations of zoning or overgrowths were recognised. Monazite with similar morphological features has also been noted (Fig. 8a, b).

Type B. Irregular grains with zones cores and unzoned rims. Cores are corroded and zoning is frequently truncated by rims (Fig. 8c, d). Again, monazite with similar appearance has been recorded. The presence of embayed zircon cores indicates it was not armoured during melting, and that dissolution was incomplete.

Type C. Equant, euhedral zircon grains with simple zoning. Very similar in appearance to the core portions of type B zircons (Fig. 8e, f). Most commonly found enclosed in biotite grains, in contrast to type A and B zircons which occur at the margins of biotite grains.

Figures 9a and b show the distribution of zircon grains of the types described above in stromatic migmatite samples KM-94-1 and KM-94-4. No accessory phases were recorded within leucosome veins or patches (nine sections from four samples). Type A accessory phases were only found at (or very near to) the leucosome-melanosome contact in stromatic migmatites. Type B accessory phases are common in the melanosome, but were not identified in leucosome or mesosome portions of the migmatites, while type C zircons only occur in the mesosome, at a distance from the melansome. The high concentration of zircon and monazite in the melanosome and absence of accessory phases in the leucosome is consistent with the mass balance calculations earlier – leucosomes have low absolute REE totals and REE are hosted only in major phases (K-feldspar and plagioclase), while melanosome REE patterns are dominated by accessory phases and REE abundances (and Zr) are much higher.

Truncation of internal zones by the growth of new rims (type B zircons) indicates that, at the temperatures of melting in the Kirtomy migmatites, intra-crystalline diffusion of Zr was slower than the rate at which zircon dissolved into the melt. Bea (1991) developed a model for this type of disequilibrium melting which he termed non-diffusive melting. In this model, partitioning of an element (e.g. Zr) between a carrier mineral (e.g. zircon) and melt is controlled solely by the extent to which the carrier mineral dissolves in the melt. This enriched layer would saturate melt in the trace element concerned – in the case of the KMS the melt-crystal interface has been enriched in Zr with the consequent growth of new zircon only at the melt-solid interface. New zircon growth is restricted to the boundary between melt and residual zircon. An idealised concentration-distance profile for a trace element at the melt-solid interface (e.g. Fig. 10 in Bea, 1991) shows that, at the onset of melting, a strongly enriched layer occurs.

The amount of zircon dissolution that occurs during anatexis, and therefore the melt Zr content, will be controlled by the zircon content of the source rocks, the temperature at which the melt forming reaction occurs, the water content of the melt, the extent to which zircon grains are armoured in stable restitic phases (Bea et al.

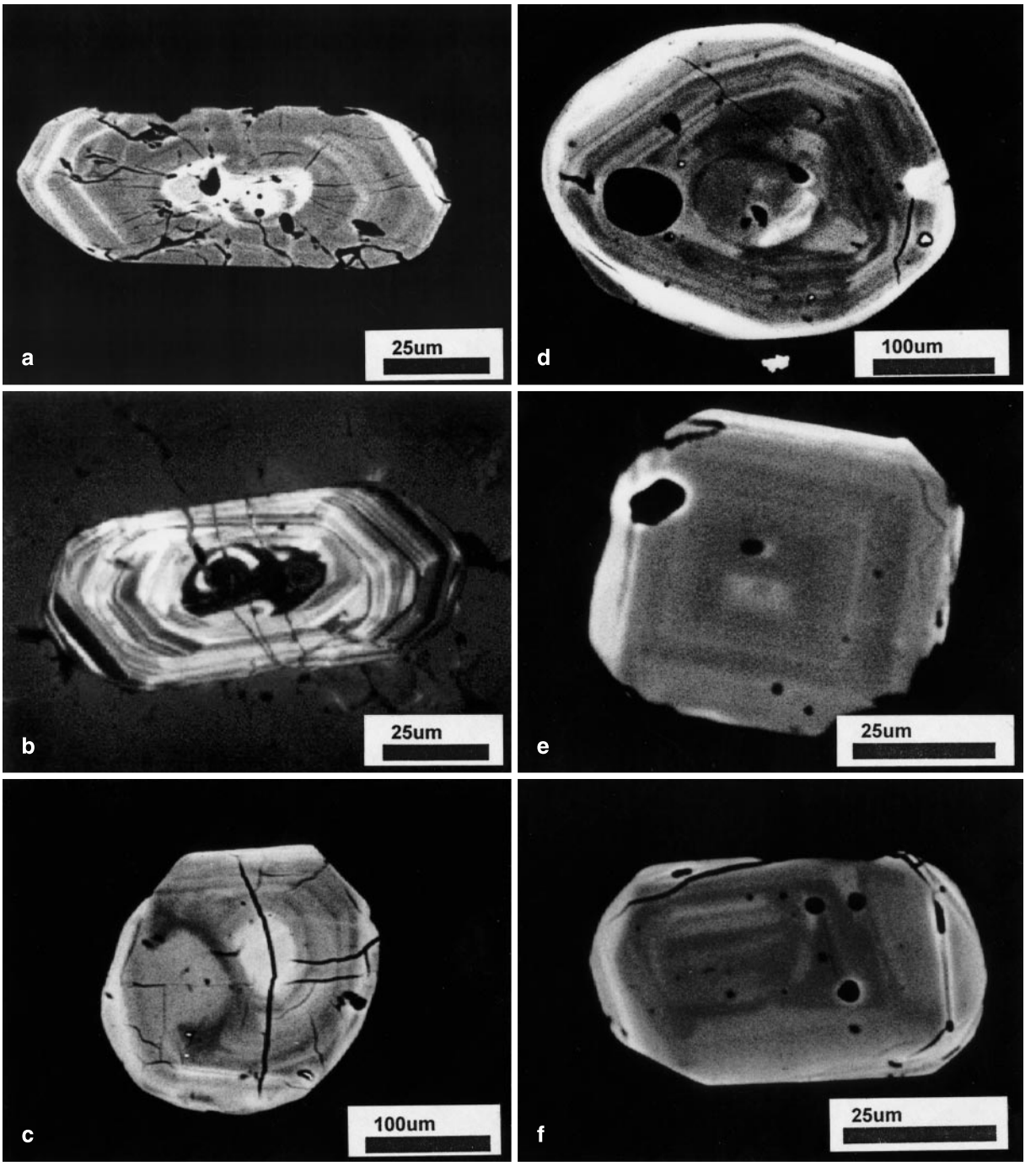

Fig. 8a–f Zircon morphology: **a** type A zircon, back-scattered electron image (BEI); **b** cathodoluminescence image of same grain; **c, d** type B zircon (both BEI); **e, f** type C zircon (both BEI). For explanation of different morphologies refer to text

1994) and the rate at which melt is removed from the melting zone. The majority of crustal lithologies contain sufficient zircon to saturate a melt in Zr, and mesosome Zr contents are comparable with typical semi-pelitic lithologies (Taylor and McClellan 1985). The concentration of partially dissolved zircons and monazites in KMS melanosomes shows that accessories were not entirely armoured during the melting event, yet they failed to dissolve completely. Zircon and monazite grains are located both at biotite margins and as inclusions, so it is unlikely that the restricted Zr and LREE concentrations of the leucosomes in stromatic migmatities are due solely to armouring. Temperatures of melting are low (700° C), restricting zircon and monazite dissolution, while the generation of felsic, water-saturated melts (indicated by the stability of biotite throughout melting) should enhance accessory phase dissolution (Watson and Harrison 1983). The exact balance of these factors is not fully understood, but dissolution rates calculated by Watson

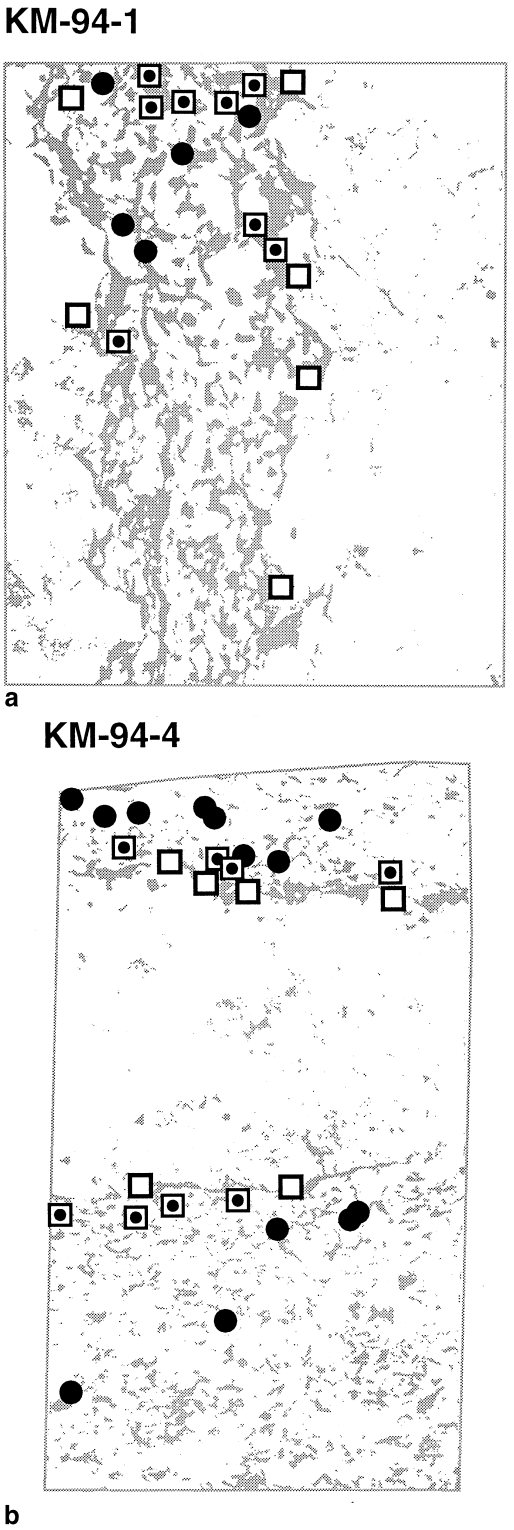

Fig. 9a, b Location of zircon types in stromatic migmatites KM-94-1 and KM-94-4. (*Open squares* type A zircon, *dotted square* type B zircon, *filled circle* type C zircon)

(1988) show a much greater dependence upon melt water content than on temperature. According to the calculations of Watson, zircon dissolution is 6 orders of magnitude more rapid in water-saturated melts at 700° C than in dry melts at the same temperature. The conditions of formation of the KMS leucosomes indicate that equilibrium melt compositions could have been generated if melt had remained in contact with melanosome for even a short period of time (>c. 10,000 years). Disequilibrium melt compositions could only have been generated if melt was extracted from melanosome over a shorter time-scale than this. Water-saturated granitic melts have relatively large viscosities compared to basaltic liquids, and the widely accepted mechanism invoked to explain rapid movement of these liquids involves the application of heterogeneous deformation and deformation-enhanced melt extraction (Sawyer 1994).

Melt extraction and disequilibrium melt geochemical signatures

Brown (1994a) argues that equilibrium melt compositions will occur in amphibolite-facies stromatic migmatities because the ΔV of the reaction is negative. This is clearly at odds with the REE and Zr chemistry of leucosomes in stromatic migmatites seen in the Kirtomy Migmatite Suite. Brown's model may only be applicable to migmatites which are forming in the absence of any applied stress – when deformation accompanies melting, melt migration (even in water-saturated migmatites) can be rapid and produce a very distinctive chemical and petrographic signature in both melt and restite (e.g. Brown 1994b). The positive Eu anomalies and low Zr contents of the Kirtomy Migmatites are more consistent with a rapid melt segregation involving rheologically driven, porous-media flow, filter pressing which can produce leucosomes in stromatic migmatites in migmatites several orders of magnitude more quickly than by pure compaction. In the concordant and discordant leucosomes of the KMS a characteristic geochemical signature manifests itself in high LREE and HREE, and also (although to a lesser extent) Zr in the melanosome and a complementary depletion of these elements in the melt.

Leucosomes in the KMS have very distinctive REE patterns when compared to leucosomes from other amphibolite-facies migmatities, and also to peraluminous granites (Carrington and Watt 1995). Peraluminous granite batholiths (e.g. Miller and Mittlefehldt 1983; Holtz and Barbey 1991) and amphibolite-facies leucosomes (Brown 1979; Sevigny et al. 1989) generally have flat to moderately fractionated REE curves and negative Eu anomalies. If removal of melt from the melting area is always rapid when it is driven by deformation, then the implications for granite chemistry are important, because granulite-facies migmatites are thought to represent the source of peraluminous granites. The melt distribution features witnessed in the Kirtomy Migmatite Suite (melt migration into structurally controlled areas

such as boudin necks and shear zones) are identical to those seen in migmatites produced by partial melting under water-undersaturated conditions. If melt extraction rates exceed melt generation rates (as theoretical considerations and field observations suggest – Sawyer 1994) in water-undersaturated migmatite complexes, then melt from granulite-facies migmatites will have REE patterns similar to those witnessed in the Kirtomy Migmatites, and which contrast with those of high level peraluminous granitoids (Carrington and Watt 1995).

Summary and conclusions

The Kirtomy Migmatite Suite (KMS) of Sutherland, Scotland, contains abundant field evidence for channelised flow and deformation-enhanced melt segregation on a hand specimen and outcrop scale (melt filled boudin necks, veins, micro-shears). Leucosomes in the KMS have low Zr contents and positive Eu anomalies which can be ascribed to disequilibrium melting and removal of leucosome before complete equilibration with source due to the inhibited dissolution of Zr and LREE. Deformation enhanced melt extraction has produced stromatic and ponded leucosomes with a characteristic trace element chemistry dominated by major phase breakdown – little or no equilibration has occurred between melt and accessory phases over the melt generation time-scale. Detailed back-scattered electron imaging shows that accessory phases were not armoured during melting, so limited accessory phase dissolution was caused by rapid, deformation driven, melt migration. Zircon morphologies and distribution are consistent with early stage non-diffusive melting models (Bea 1991) which predict a trace element build up at the melt-residue interface when trace element diffusion rates in minerals are slower than mineral dissolution. Coexisting melanosomes show a corresponding increase in Zr and LREE reflecting the concentration of refractory accessories in residual material during disequilibrium melting.

Acknowledgements This work was carried out thanks to the support of Oxford Brookes University – G.R.W. wishes to acknowledge the award of funding from the Scholarship Fund and I.M.B. the funding provided for his PhD. Mike Brown and an anonymous reviewer are thanked for their constructive criticism which improved the paper greatly. Many thanks to Nanny and James Allen in Bettyhill for the warm hospitality, to Andy Hume and Al Matthewson for their help in the field, Chris Gilbert for the ICP analysis, John Craven and Richard Hinton at Edinburgh for help with the unpublished SIMS analyses and Clark Friend, Mike Fowler, Richard D'Lemos, Rob Strachan, Ian Tribe and Anton Kearsley for comments and advice on the manuscript.

References

Ashworth JR, Brown M (1990) An overview of diverse responses to diverse processes at high crustal temperatures. In: Ashworth JR, Brown M (eds) High-temperature metamorphism and crustal anatexis. Unwin Hyman, London, pp 1–18

Barbey P, Macaudiere J, Nzenti JP (1990) High pressure dehydration melting of metapelites: evidence from the migmatites of Yaoundé. J Petrol 31: 401–427

Bea F (1991) Geochemical modelling of low melt fraction anatexis in a peraluminous system: the Peña Negra Complex (central Spain). Geochim Cosmochim Acta 55: 1859–1874

Bea F, Pereira MD, Stroh A (1994) Mineral/leucosome trace element partitioning in a peraluminous migmatite (a laser ablation-ICPMS study). Chem Geol 117: 291–312

Bedard JH (1989) Disequilibrium mantle melting. Earth Planet Sci Lett 91: 359–366

Brown M (1979) The petrogenesis of the St Malo migmatite belt, Armorican Massif, France, with particular reference to the diatexites. Neues Jahrb Mineral Abh 135: 48–74

Brown M (1994a) Melt segregation mechanism controls on the geochemistry of crustal melts (abstract). Mineral Mag 58a: 124–125

Brown M (1994b) The origin of migmatites (abstract). The controls of metamorphism – University of Liverpool 5

Brown M, Averkin YA, McLellen EL (1995a) Melt segregation in migmatites. J Geophys Res 100: 15655–15679

Brown M, Rushmer T, Sawyer EW (1995b) Introduction to special section: mechanisms and consequences of melt segregation from crustal protoliths. J Geophys Res 100: 15551–15563

Burns IM (1994) Tectonothermal evolution and petrogenesis of the Naver and Kirtomy Nappes, north Sutherland, Scotland (unpublished). PhD thesis, Oxford Brookes Univ

Campbell IH, Gorton MP (1980) Accessory phases and the generation of LREE-enriched basalts – a test for disequilibrium melting. Contrib Mineral Petrol 72: 157–163

Carrington DP, Watt GR (1995) A geochemical and experimental study of the role of K-feldspar during water-undersaturated melting of metapelites. Chem Geol 122: 56–79

Clemens JD (1990) The granulite-granite connexion. In: Vielzeuf D, Vidal Ph (eds) Granulites and crustal evolution. Kluwer Academic Publishers, Dordrecht, pp 25–36

Clemens JD, Vielzeuf D (1987) Constraints on melting and magma production in the crust. Earth Planet Sci Lett 86: 287–306

France-Lanord C, Le Fort P (1988) Crustal melting and granite genesis during the Himalayan collision orogenesis. Trans Roy Soc Edinburgh 79: 209–222

Graham CM, Powell R (1984) A garnet-hornblende geothermometer: calibration, testing, and application to the Pelona Schist, Southern California. J Metamorphic Geol 2: 13–31

Harris N, Ayres M, Massey J (1994) Chemical disequilibrium during crustal anatexis (abstract). Mineral Mag 58a: 380–381

Hinton RW (1990) Ion microprobe analysis of silicates; measurements of multi-element glasses. Chem Geol 83: 11–25

Hinton RW, Upton BGJ (1991) The chemistry of zircon: variations within and between large crystals from syenite and alkali basalt xenoliths. Geochim Cosmochim Acta 55: 3287–3302

Holdsworth RE, Strachan RA, Harris AL (1995) Precambrian rocks in northern Scotland east of the Moine Thrust: the Mointe Supergroup. In: Gibbons W, Harris AL (eds) A revised correlation of Precambrian rocks in the British Isles. Geol Soc London Spec Rep 22, pp 23–32

Holland T, Blundy J (1994) Non-ideal interactions in calcic amphiboles and their bearing on amphibole-plagioclase thermometry. Contrib Mineral Petrol 116: 433–447

Holtz F (1989) Importance of melt fraction and source rock composition in crustal genesis – the example of two granitic suites of northern Portugal. Lithos 24: 21–35

Holtz F, Barbey P (1991) Genesis of peraluminous granites. II. Mineralogy and chemistry of the Tourem Complex (north Portugal): sequential melting versus restite unmixing. J Petrol 32: 959–978

Holtz F, Johannes W (1994) Maximum and minimum water contents of granitic melts: implications for chemical and physical properties of ascending magmas. Lithos 32: 149–159

Iwamori H (1994) Dynamic disequilibrium melting model with porous flow and diffusion controlled chemical equilibration. Earth Planet Sci Lett 114: 301–313

Johannes W (1978) Melting of plagioclase in the system Ab-An-H_2O and Qz-Ab-An-H_2O at P_{H_2O}=5 kbar, an equilibrium problem. Contrib Mineral Petrol 66: 295–303

Johannes W (1980) Metastable melting in the granite system Qz-Or-Ab-An-H_2O. Contrib Mineral Petrol 72: 73–80

Kohn MJ, Spear FS (1990) Two new geobarometers for garnet amphibolites, with applications to Southeastern Vermont. Am Mineral 75: 89–96

McLellan EL (1988) Migmatite structures in the Central Gneiss Complex, Boca de Quadra, Alaska. J Metamorphic Geol 6: 517–542

Miller CF (1985) Are strongly peraluminous magmas derived from pelitic sedimentary sources. J Geol 93: 673–689

Miller CF, Mittlefehldt DW (1983) Geochemistry of the Sweetwater Wash Pluton, California: implications for "anomalous" trace element behaviour during differentiation of felsic magmas. Geochim Cosmochim Acta 47: 109–124

Montel JM (1993) A model for monazite/melt equilibrium and application to the generation of magmas. Chem Geol 100: 127–146

Nabelek PI, Glascock MD (1995) REE-depleted leucogranites, Black Hills, South Dakota: a consequence of disequilibrium melting of monazite-bearing schists. J Petrol 36: 1055–1071

Naslund HR (1986) Disequilibrium melting and rheomorphic layer formation in the contact aureole of the Basistoppen sill, East Greenland. Contrib Mineral Petrol 93: 359–367

Paterson SR, Tobisch OT (1992) Rates of processes in magmatic arcs: implications for the timing and nature of pluton emplacement and wall rock deformation. J Struct Geol 14: 291–300

Patiño-Douce AE, Johnston AD (1991) Phase equilibria and melt productivity in the pelitic system: implications for the origin of peraluminous granitoids and aluminous granulites. Contrib Mineral Petrol 107: 202–218

Pattison DRM, Harte B (1988) Evolution of structurally contrasting anatectic migmatites in the 3-kbar Ballachulish aureole, Scotland. J Metamorphic Geol 6: 475–494

Qin Z (1992) Disequilibrium partial melting model and its implications for trace element fractionations during mantle melting. Earth Planet Sci Lett 112: 75–90

Sawyer EW (1991) Disequilibrium melting and the rate of melt-residuum separation during migmatisation of mafic rocks from the Grenville Front, Quebec. J Petrol 32: 701–738

Sawyer EW (1994) Melt segregation in the continental crust. Geology 22: 1019–1022

Sevigny JH, Parrish RR, Ghent ED (1989) Petrogenesis of peraluminous granites, Monashee Mountains, southeastern Canadian Cordillera. J Petrol 30: 557–581

Srogi L, Wagner ME, Lutz TM (1993) Dehydration partial melting and disequilibrium melting in the granulite-facies Wilmington Complex, Pennsylvania-Delaware Piedmont. Am J Sci 293: 405–465

Taylor SR, McClennan SM (1985) The continental crust: its composition and evolution. Blackwell, Oxford

Vielzeuf D, Holloway JR (1988) Experimental determination of the fluid-absent melting reactions in the pelitic system. Contrib Mineral Petrol 98: 257–276

Watkins PJ, Nolan J (1992) Determination of rare-earth elements, scandium, yttrium and hafnium in 28 geochemical reference materials using inductively coupled plasma atomic emission spectrometry. Chem Geol 95: 131–139

Watson EB (1988) The role of accessory minerals in granitoid geochemistry (abstract). The origin of granites. Roy Soc Edinburgh Roy Soc London Hutton Meet, Edinburgh, pp 19–20

Watson EB, Harrison TM (1983) Zircon saturation revisited: temperature and compositional effects in a variety of crustal magma types. Earth Planet Sci Lett 64: 295–304

Watt GR, Harley SL (1993) Accessory phase controls on the geochemistry of crustal melts and restites produced by dehydration melting. Contrib Mineral Petrol 114: 550–566

Weber C, Barbey P, Cuney M, Martin H (1985) Trace elements behaviour during migmatisation: evidence for a complex melt-residuum-fluid interaction in the St. Malo migmatitic dome (France). Contrib Mineral Petrol 90: 52–62

White AJR (1990) A workshop on crustal protoliths of granites: course notes. Dep Geol, Univ St Andrews, Scotland

Zinner E, Crozaz G (1987) A method for the quantitative measurement of rare earth elements in the ion microprobe. In J Mass Spectrom Ion Phys 69: 17–38